Materials and Manufacturing Processes, 31: 359–365, 2016

ISSN: 1042-6914 print/1532-2475 online
DOI: 10.1080/10426914.2015.1058952

Effect of TiO_2 Crystalline Phase on Performance of Flux Assisted GTA Welds

Kuang-Hung Tseng and Po-Yuan Chen

Institute of Materials Engineering, National Pingtung University of Science and Technology, Pingtung, Taiwan

Rutile and anatase TiO_2 fluxes were used to investigate the influence of the powdered oxides on the joint penetration ability (JPA) and solidification cracking susceptibility (SCS) in the gas tungsten arc (GTA) welding of type 316L stainless steel (SS). The mechanisms underlying the increase in JPA of GTA welds made with various crystalline phases of TiO_2 were also identified. The results indicate that GTA welding with rutile TiO_2 (R-TiO_2) or anatase TiO_2 (A-TiO_2) forms a viscous slag over the surface of the weld. The R-TiO_2 is more thermodynamically stable than the A-TiO_2, leading to a greater improvement in JPA of GTA weld made with A-TiO_2. The welding arc action can be ignored and only the convection of the molten pool should be considered in the underlying mechanism for the increase in JPA of GTA weld made with R-TiO_2 or A-TiO_2. Moreover, the TiO_2 assisted GTA welding of type 316L SS was effective in decreasing the SCS.

Keywords Additives; Anantase; Flux; Oxide; Powder; Rutile; Titania; Welding.

Introduction

Gas tungsten arc (GTA) welding is extensively used for joining thin sections of metals as it produces high-quality welds. The limited depth of the GTA weld necessitates the use of edge beveling preparations and the addition of filler metals for joining metals more than 2.5 mm thick [1, 2]. The use of a flux that increases the depth of the GTA welds was developed by the E. O. Paton Electric Welding Institute in the mid-1960s, and was termed flux assisted GTA welding. This process was initially intended for welding titanium alloys, before being applied to steels. The first publication describing the flux assisted GTA welding of titanium alloys was in 1965 [3], and the first paper describing the flux assisted GTA welding of steels was in 1968 [4]. The main advantage of using a flux is a reduction in the thermal energy required for GTA welding of thick sections of metals [5]. The flux assisted GTA welding normally results in a 200–300% increase in the depth of the weld [6], thereby increasing productive efficiency in GTA welding.

Tathgir et al. [7] reported that TiO_2 increased the depth of AISI 1020 carbon steel GTA weld. Modenesi et al. [8] studied the influence of fluxes on the weld geometry in GTA welding of AISI 304 stainless steel (SS), and showed that TiO_2, SiO_2, Fe_2O_3, and AlF_3 increased the depth of the weld, whereas CaF_2 and Al_2O_3 had no effect on the depth, as compared to the conventional GTA weld. Lin and Wu [9] reported that SiO_2, NiO, MoS_2, MoO_3, Cr_2O_3, TiO_2, and ZnO produced a high depth of 718 nickel-base alloy GTA weld. Qin et al. [10] reported that the use of TiO_2 led to a full joint penetration in the 6013 aluminum alloy CO_2 laser weld, and that TiO_2 gave the greatest improvement in the absorption of laser welding energy. Sun et al. [11] reported that TiO_2, SiO_2, and Cr_2O_3 increased the depth of AZ31B magnesium alloy Nd:YAG laser weld. It can be seen that TiO_2 is widely used for the flux assisted GTA welding of ferrous and nonferrous metals. The two most common and important crystalline phases of TiO_2 are rutile and anatase. Rutile TiO_2 (R-TiO_2) is the most thermodynamically stable phase at all temperatures, while anatase TiO_2 (A-TiO_2) is a metastable phase that can be transformed to the rutile phase when heated [12].

Researchers have diametrically various opinions as to the mechanism leading to the increased the depth of the flux assisted GTA welds [6, 13]. Some researchers are of the opinion that the constriction of the welding arc increases the electromagnetic force within the molten pool, thus increasing the depth of the weld. Other researchers have proposed that the main cause of the high depth of the weld lies in the change in the tension temperature gradient ($\Delta\gamma/\Delta T$) on the surface of the molten pool of metal, from falling to rising, thus reversing the direction of the induced thermocapillary force. The crystalline phase of TiO_2 is a key factor in determining the depth of the TiO_2 assisted GTA weld, and is of much interest in research [6]. The causes for the variation in the depth of GTA welds when various crystalline phases of TiO_2 are used, as well as solidification cracks in the GTA weld when a flux is used, have been studied less frequently. The solidification cracking is one of the major defects in the fusion welding of SS. More research to understand the action of the TiO_2 crystalline phase used in the flux assisted GTA welding of austenitic SS

Received March 19, 2015; Accepted May 14, 2015

Address correspondence to Kuang-Hung Tseng, Institute of Materials Engineering, National Pingtung University of Science and Technology, Pingtung 91201, Taiwan; E-mail: tkh@mail.npust.edu.tw

Color versions of one or more of the figures in the article can be found online at www.tandfonline.com/lmmp.

is therefore required. In this study, two types of TiO_2 crystalline phases are used to investigate the influence of powdered oxides on the joint penetration ability (JPA) and solidification cracking susceptibility (SCS) in the TiO_2 assisted GTA welding of type 316L SS. This study also attempts to elucidate the integrated mechanism that causes an improvement in the depth of GTA welds made with various crystalline phases of TiO_2, through analyzing data from the current experiment.

Materials and methods

Type 316L SS with a chemical composition (in wt.%) of 0.02% C, 0.86% Mn, 0.50% Si, 0.025% P, 0.003% S, 17.1% Cr, 12.1% Ni, 2.08% Mo, 0.05% N, 0.28% Cu, and the remainder Fe was selected as the specimen. The dimensional designation of the specimen was $150 \times 150 \times 6$ mm. Two types of powdered oxides (R-TiO_2 and A-TiO_2) were selected as the flux. Table 1 shows the properties of powdered TiO_2. Figure 1 shows the operating procedure of the TiO_2 assisted GTA welding. 1000 mg of powdered TiO_2 was mixed with 1.5 mL of methanol and stirred with a rod until the mixture formed a paste, which was subsequently coated onto the surface of the specimen with a 12 mm-wide flat brush. The weight per unit coated area of the TiO_2 layer was 2.32 mg/cm^2 and the drying time of the coated layer was 1 min.

The GTA bead-on-plate welding trial was performed using a semi-automatic torch with a 3.2 mm diameter, 60° included angle, 1.5% lanthanated tungsten electrode (AWS classification EWLa-1.5). To maintain consistency in the TiO_2 assisted GTA welding operation, a special setup was designed to conduct the welding. Two specimens were clamped next to each other with a 2.5 mm gap, in order to prevent any thermal conduction between these two specimens. The first specimen was a normal one without TiO_2, while the second specimen was coated with TiO_2. The torch ran from the first specimen to the second specimen without interruption, thus allowing GTA welding with and without TiO_2 to be performed under identical conditions. The travel speed and welding current were 140 mm/min and 180 A, respectively. The arc length was fixed at 2 mm prior to welding using a feeler gauge. Argon gas was supplied through the torch at a flow rate of 12 L/min. A gas nozzle has an exit diameter of 12.8 mm. During welding, two charge-coupled device (CCD) detectors were used to monitor both the arc column and the anode spot (Fig. 2).

The spot-varestraint test (SVT) is a weldability testing technique. The SVT was conducted on the GTA spot-on-plate weld, allowing for the quantification of the SCS. A stationary GTAW torch was used to produce a spot weld in the center of the specimen. After the weld was established for a predetermined time, the specimen was forced around a curved die block and the arc was extinguished. Solidification cracks formed radially around the fusion zone. In this evaluation, the maximum crack length (MCL), total crack length (TCL), and total number of cracks (TNC) were quantified on the fusion zone of a spot-on-plate weld. Figure 3 shows a schematic of SVT for evaluating the SCS. The dimensional designation of the specimen was $250 \times 50 \times 3$ mm. Each specimen was subjected to one spot weld at 110 A for 6 s, and was subsequently conducted at an imposed strain of 5%. The arc length was fixed at 2 mm. The flow rate of argon gas was 12 L/min. After testing, the crack lengths were measured using a Toolmaker's microscope.

The as-welded appearance was photographed using a stereoscopic microscope, and the weldment was subsequently cross-sectioned, mounted, ground, and polished, followed by etching with 10 g $H_2C_2O_4 + 100$ mL H_2O solution to reveal the weld profile, in accordance to standard metallographic procedures. The weld profile was photographed using an optical microscope, and the weld depth (D) and bead width (W) were measured using a Toolmaker's microscope. The readings were measured at three sections of the weld and the average value was calculated. In addition, the ferrite content (FC) of the weld metal was measured using a feritscope. The oxygen concentration (OC) in the weld metal was measured using an oxygen/nitrogen/hydrogen analyzer.

Table 1.—Properties of powdered TiO_2 used in this study.

Properties	Powdered oxide	
	R-TiO_2	A-TiO_2
Crystal structure	Tetragonal (a: 0.4584 nm; c: 0.2953 nm)	Tetragonal (a: 0.3733 nm; c: 0.9370 nm)
Particle size	73 ± 5 μm	74 ± 4 μm
Mass density	4.23 g/cm^3	3.78 g/cm^3
Refractive index	2.75	2.54
Melting point	1843°C	converts to rutile
Band-gap	3.03 eV	3.20 eV

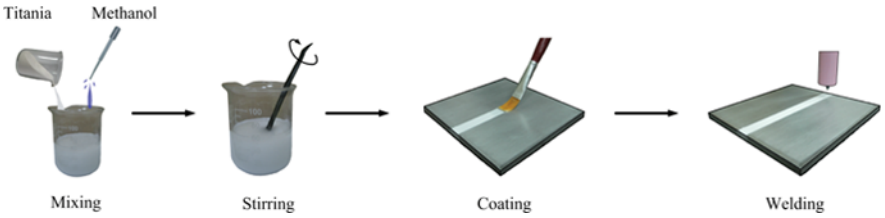

Figure 1.—Operating procedure of TiO_2 assisted GTA welding.

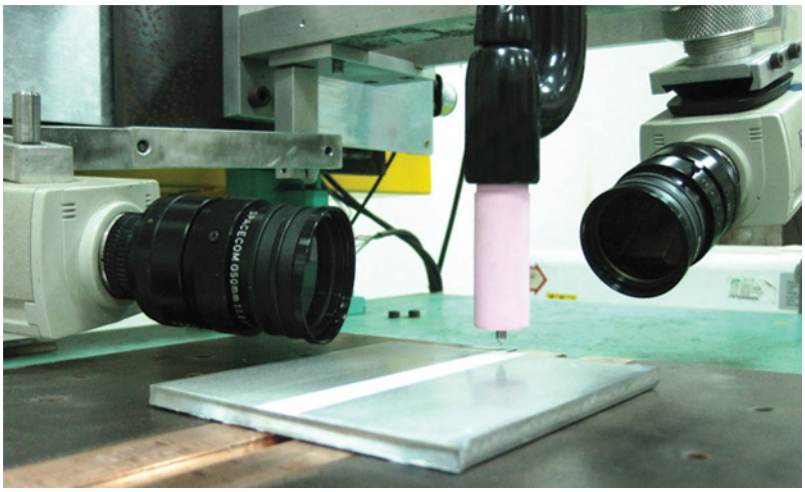

FIGURE 2.—CCD detectors for monitoring arc column and anode spot.

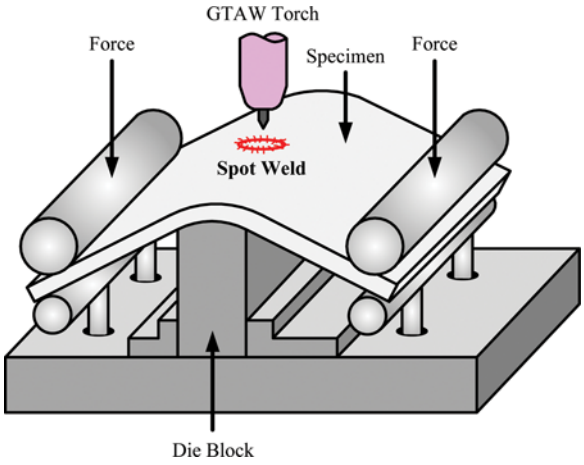

FIGURE 3.—Spot-varestraint test for evaluating solidification cracking susceptibility.

RESULTS AND DISCUSSION

Appearance and shape of the welds are quality indicators of the flux assisted GTA welding. Figure 4 shows the surface appearance of GTA welds made with and without TiO_2. GTA weld made without TiO_2 produced a clean, spatter-free surface with a metallic luster. The use of R-TiO_2 produced approximately $13.5 \pm 0.2\%$ as-welded surface coverage of slag and a few spatters, while the use of A-TiO_2 produced a relatively small quantity of slag (approximately as-welded surface coverage of $8.4 \pm 0.1\%$) and was spatter-free. It was concluded that for this case observed in this work, GTA weld made with R-TiO_2 or A-TiO_2 tends to form a viscous slag over the as-welded surface.

It is also evident from Fig. 4 that GTA weld made without TiO_2 has a shallow, wide shape, while GTA welds made with R-TiO_2 and A-TiO_2 have a deep, narrow shape. The shape of the weld is often described in terms of a weld D/W. GTA welding without TiO_2 produced a weld D/W of 0.14. GTA welding with R-TiO_2 or A-TiO_2 is capable of increasing the weld D/W, with the magnitude of the increase depending on the crystalline phase of TiO_2. In this case, the use of R-TiO_2 produced a weld D/W of 0.68, while the use of A-TiO_2 produced a weld D/W of 0.74.

Compared to GTA weld made without TiO_2, there is a dramatic increase in the depth of GTA weld made with TiO_2. The constricted column of the welding arc or reversed convection in the molten pool has been proposed as the underlying mechanism for the increased depth of the flux assisted GTA weld. However, these explanations have divided scientific opinion, and have been discussed individually in other papers. This study provides an interpretation of the integrated mechanism that causes an increase in depth of the flux assisted GTA welds.

Figure 5 shows the arc column and anode spot for GTA welding with and without TiO_2. This photograph is a combination of the arc column (welding arc part) and the anode spot (molten pool part). It was created using image synthesis hardware. The results indicated that the arc column and anode spot for GTA welding with TiO_2 are constricted compared to GTA welding without TiO_2. TiO_2 is a wide band-gap insulator with high dielectric constant [14]. Although the electrical resistivity of the oxides decreases rapidly as the heating temperature increases [15], the electrical resistivity of TiO_2 ($1.2 \times 10^7\ \Omega \cdot cm$) is significantly higher than that of molten iron ($1.4 \times 10^{-4}\ \Omega \cdot cm$). During GTA welding, the heating temperature in the inner core of the welding arc is high enough to melt TiO_2, such that the arc heat can be transferred to the molten pool. At the same time, under the action of the plasma jet, the unmelted TiO_2 particles will be forced out to the peripheral region of the molten pool surface and to the adjoining region of the base metal. During the TiO_2 assisted GTA welding, an insulating bond is formed at the peripheral regions of the molten pool surface, due to the large difference in

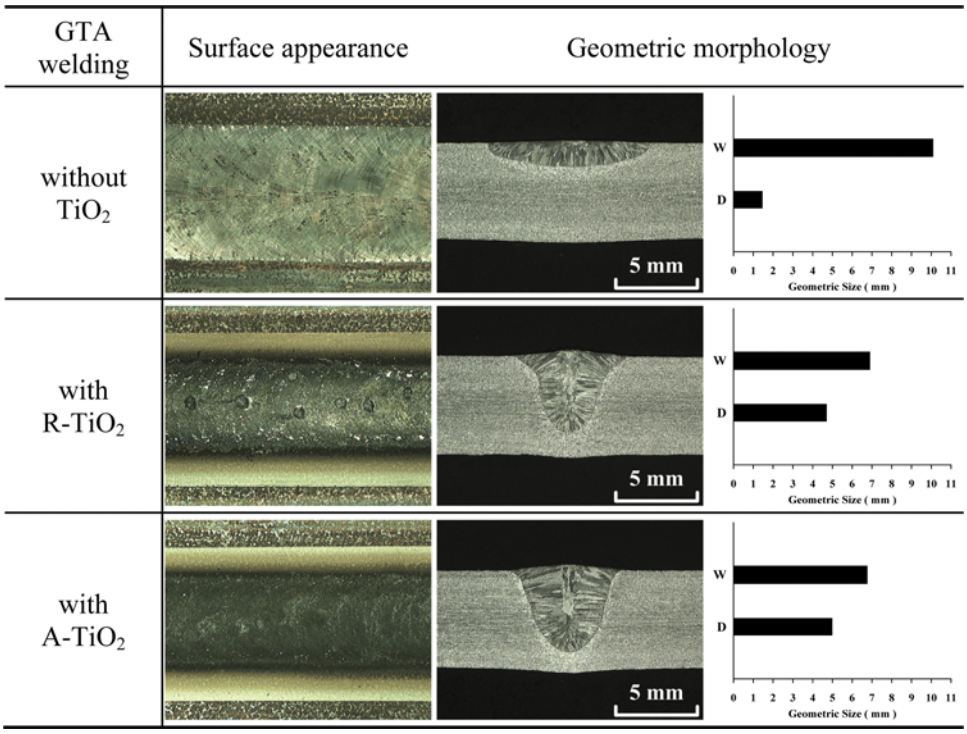

FIGURE 4.—Surface appearance and geometric morphology of GTA welds made with and without TiO_2.

electrical resistivity between the TiO_2 particles and liquid iron, thus restricting the arc current only through the central region of the molten pool. The restriction in the electrically conducting channel of the welding arc results in an increase in current density at the anode spot [15], leading to an increase in the electromagnetic force within the molten pool. The electromagnetic force dominates a downward flow of liquid metal within the molten pool. The results promote an effective energy of arc heat transfer from the surface of the molten pool to its bottom.

The dissolved oxygen within the molten pool arising from the decomposition of the oxide is a key factor in determining the convection circulation of the thermocapillary force. The thermocapillary force dominates an inward or outward convection of liquid metal along the surface of the pool of molten metal. Based on a previous study [16], when the OC in the 304 SS weld metal was greater than 70 ppm, the value of $\Delta\gamma/\Delta T$ was positive. In this case, an inward convection of liquid metal along the surface of the molten pool (called the reversed thermocapillary force) occurs. The influence of the critical OC on the value of $\Delta\gamma/\Delta T$ may differ depending on the method of welding process and the composition of base metal to be welded. Figure 6 shows the average OC in type 316L SS GTA welds made with and without TiO_2. The results indicated that the average OC in type 316L SS weld metal made with TiO_2 is in the range of 57–68 ppm. Under these conditions, this study surmised that there exists sufficient dissolved oxygen within type 316L SS molten pool, such that the direction of the thermocapillary force is reversed to go inward along the pool surface of molten metal.

It was concluded that for this case examined in the present work, the combination of an increased electromagnetic force caused by a dramatic increase in current density at the anode spot together with a reversed thermocapillary force within the molten pool led to a stronger inward and downward flow of liquid metal toward the bottom of the molten pool. This results in an effective energy of arc heat transfer from the edge of the molten pool surface to its center, and then downward to the bottom of the molten pool. Consequently, a weld with a deep depth, narrow width is expected in the TiO_2 assisted GTA welding of type 316L SS.

Under the same welding parameters, the JPA of GTA welding with R-TiO_2 or A-TiO_2 was approximately 220% and 240%, respectively. The results indicated that the use of A-TiO_2 exhibits a greater improvement in JPA of GTA welding of type 316L SS compared to the ability achieved with R-TiO_2. By comparing Figs. 5(b) and 5(c), it can be observed that there was no major difference in both the arc column and the anode spot for GTA welding with R-TiO_2 or A-TiO_2. The action of the welding arc could therefore be dismissed as the underlying mechanism for the increased depth of GTA weld made with A-TiO_2 compared to R-TiO_2, and consideration was given only to the convection of the molten pool. In Fig. 6, the average OC in type 316L SS GTA weld made with A-TiO_2 was higher than that for R-TiO_2. Ogden et al. [17] reported that standard free energy of formation for R-TiO_2 was less than that of A-TiO_2; thus,

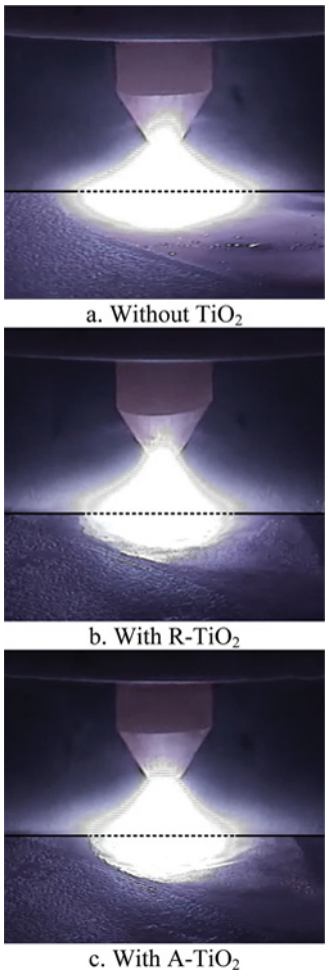

FIGURE 5.—Arc column and anode spot of GTA welding with and without TiO_2.

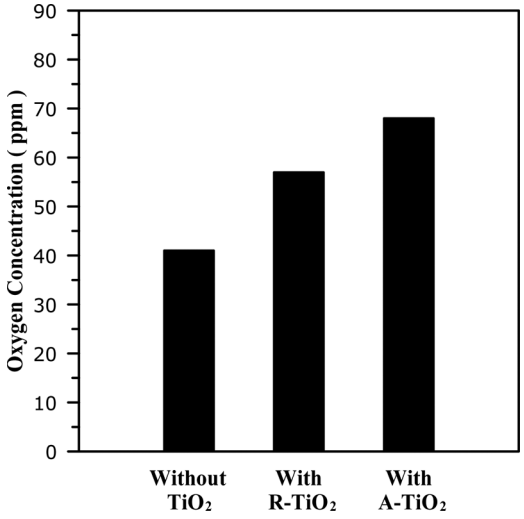

FIGURE 6.—Average oxygen concentration in GTA welds made with and without TiO_2.

R-TiO_2 was more thermodynamically stable than A-TiO_2 at all examined temperatures. This leads to difficult decomposition of R-TiO_2, resulting in the dissolved oxygen within the molten pool made with R-TiO_2 to be relatively low at the same amount of net heat. Consequently, the depth of GTA weld made with A-TiO_2 was higher than that of GTA weld made with R-TiO_2.

Ogawa and Tsunetomi [18] reported that phosphorus and sulfur combine with iron to form low-melting point compounds such as Fe_3P (1166°C) and FeS (1190°C), which in turn could form low-melting point eutectics such as Fe_3P–Fe (1050°C) and FeS–Fe (988°C). When the thermal or mechanical strain exceeds the inherent ductility of the solidifying metal or low-melting eutectics persist along the interdendritic regions or dendrite grain boundaries, this leads to the formation of solidification cracks. Figure 7 shows the location of the solidification cracks in the GTA spot-on-plate weld. The results indicated that most of the cracks discovered were located in the peripheral regions of a spot weld due to bending induced strain. In addition, the cracks were oriented along the direction of solidification and the majority was in the region that was perpendicular to the direction of the maximum imposed strain.

The index of the SCS is described as MCL, TCL, and TNC in a spot weld. Table 2 shows the SCS in the GTA spot welds made with and without TiO_2. The results indicated a reduction in MCL, TCL, and TNC with the TiO_2 assisted GTA welding of type 316L SS. Goodwin [19] reported that an increased heat input increased the SCS in the GTA welding of type 316 SS. Compared to GTA welding without TiO_2, GTA welding with TiO_2 produces a higher D/W of the weld and has a higher power density of the heat source. As the power density of the welding heat source increases, the amount of thermal energy from the arc is transferred to the workpiece that required welding decreases [20]. Table 2 also shows type 316L SS GTA weld made with TiO_2 had a higher ferrite number (FN) compared to the weld without TiO_2. The delta-ferrite (δ) phase within the austenite (γ) matrix increased the weld solidification

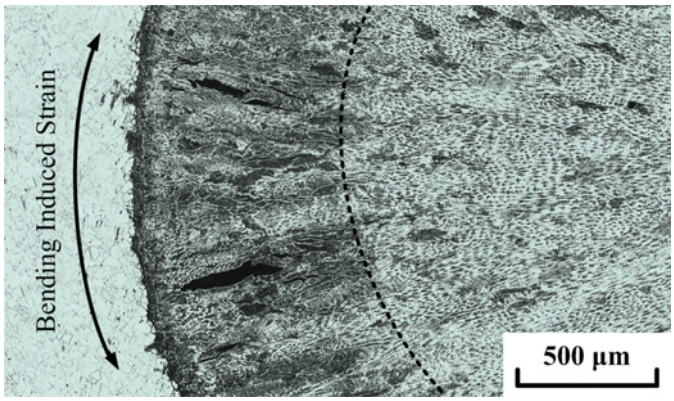

FIGURE 7.—Location of solidification cracks in GTA spot-on-plate weld.

Table 2.—Solidification cracking susceptibility of GTA welds made with and without TiO_2.

	Spot-Varestraint Test		
	Without TiO_2	With R-TiO_2	With A-TiO_2
	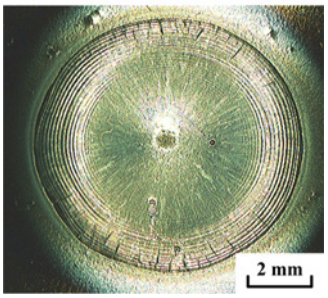	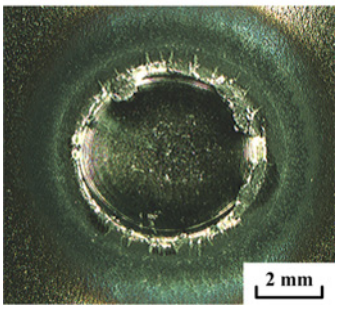	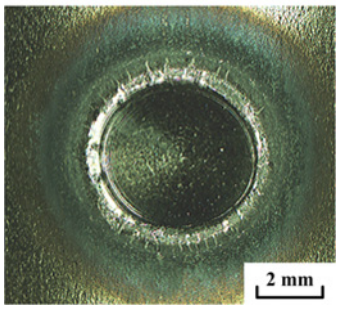
Index of SCS			
MCL	0.96 mm	0.54 mm	0.43 mm
TCL	17.74 mm	8.66 mm	6.94 mm
TNC	72	30	25
FC	4.1 ± 0.4 FN	5.9 ± 0.2 FN	6.2 ± 0.2 FN

cracking resistance. The reason for this is δ phase exhibited higher solubility of impurity elements than the γ phase. Thus, it has a beneficial effect to reduce the segregation of harmful impurities in the interdendritic regions. In addition, the δ phase embedded in the γ matrix (δ/γ interface) exhibited better wettability of grain boundaries than the δ/δ or γ/γ interface. Thus, it has a beneficial effect in reducing the concentration of harmful impurities at the dendrite grain boundaries. Consequently, the TiO_2 assisted GTA welding of type 316L SS has a remarkable effect in decreasing the SCS. The study also found that the use of R-TiO_2 or A-TiO_2 does not lead to a significant difference in SCS in the TiO_2 assisted GTA welding of type 316L SS.

Conclusions

The influences of R-TiO_2 and A-TiO_2 on the JPA and SCS in the GTA welding of type 316L SS were investigated. This study has also identified the underlying mechanisms for the increased the JPA of GTA welds made with various crystalline phases of TiO_2. The findings are summarized as follows:

1. GTA welding with R-TiO_2 or A-TiO_2 forms a viscous slag over the surface of type 316L SS weld. Compared to GTA welding with R-TiO_2, GTA welding with A-TiO_2 produced a higher D/W of the weld.
2. GTA weld made with A-TiO_2 has improved the JPA compared to GTA weld made with A-TiO_2. The reason for this is the R-TiO_2 is more thermodynamically stable than the A-TiO_2.
3. The welding arc action can be ignored and only the convection of the molten pool should be considered in the underlying mechanism for the increase in JPA of GTA weld made with R-TiO_2 or A-TiO_2.
4. The TiO_2 assisted GTA welding increases the power density of the heat source, and is thus advantageous for decreasing the solidification cracks in type 316L SS weld metal. The use of R-TiO_2 or A-TiO_2 does not lead to a significant difference in SCS.

Funding

The authors gratefully acknowledge the financial support provided to this study by the Ministry of Science and Technology (MOST), Taiwan, under grant no. 103-2622-E-020-007-CC3.

References

1. Tseng, K.H.; Chen, K.L. Comparisons between TiO_2- and SiO_2-flux assisted TIG welding processes. *Journal of Nanoscience and Nanotechnology* **2012**, *12* (8), 6359–6367.
2. Tseng, K.H.; Chuang, K.J. Application of iron-based powders in tungsten inert gas welding for 17Cr-10Ni-2Mo alloys. *Powder Technology* **2012**, *228*, 36–46.
3. Gurevich, S.M.; Zamkov, V.N.; Kushnirenko, N.A. On improving the effectiveness of titanium welds in argon-arc welding. *Avtomaticheskaya Svarka* **1965**, (9), 1–4.
4. Makara, A.M.; Kushnirenko, B.N.; Zamkov, V.N. Argon-arc flux welding of high-strength martensitic steel. *Avtomaticheskaya Svarka* **1968**, (*7*), 73–74.
5. Tseng, K.H. Development and application of oxide-based flux powder for tungsten inert gas welding of austenitic stainless steels. *Powder Technology* **2013**, *233*, 72–79.
6. Sándor, T.; Mekler, C.; Dobránszky, J.; Kaptay, G. An improved theoretical model for A-TIG welding based on surface phase transition and reversed Marangoni flow. *Metallurgical and Materials Transactions A* **2013**, *44* (1), 351–361.

7. Tathgir, S.; Bhattacharya A.; Bera, T.K. Influence of current and shielding gas in TiO_2 flux activated TIG welding on different graded steels. *Materials and Manufacturing Processes* **2015**, *30* (9), 1115–1123.
8. Modenesi, P.J.; Apolinário, E.R.; Pereira, I.M. TIG welding with single- component fluxes. *Journal of Materials Processing Technology* **2000**, *99* (1–3), 260–265.
9. Lin, H.L.; Wu, T.M. Effects of activating flux on weld bead geometry of Inconel 718 alloy TIG welds. *Materials and Manufacturing Processes* **2012**, *27* (12), 1457–1461.
10. Qin, G.L.; Wang, G.G.; Zou, Z.D. Effects of activating flux on CO_2 laser welding process of 6013 Al alloy. *Transactions of Nonferrous Metals Society of China* **2012**, *22* (1), 23–29.
11. Sun, H.; Song, G.; Zhang, L.F. Effects of oxide activating flux on laser welding of magnesium alloy. *Science and Technology of Welding and Joining* **2008**, *13* (4), 305–311.
12. Hu, Y.; Tsai, H.L.; Huang, C.L. Effect of brookite phase on the anatase-rutile transition in titania nanoparticles. *Journal of the European Ceramic Society* **2003**, *23* (5), 691–696.
13. Tseng, K.H.; Wang, N.S. GTA welding assisted by mixed ionic compounds of stainless steel. *Powder Technology* **2014**, *251*, 52–60.
14. Takata, S.; Miura, Y.; Matsumoto, Y. Evidence for the intrinsic nature of band-gap states electrochemically observed on atomically flat TiO_2(110) surfaces. *Physical Chemistry Chemical Physics* **2014**, *16*, 24784–24789.
15. Lowke, J.J.; Tanaka, M.; Ushio, M. Mechanisms giving increased weld depth due to a flux. *Journal of Physics D: Applied Physics* **2005**, *38* (18), 3438–3445.
16. Tseng, K.H.; Lin, P.Y. UNS S31603 stainless steel tungsten inert gas welds made with microparticle and nanoparticle oxides. *Materials* **2014**, *7* (6), 4755–4772.
17. Ogden, A.; Corno, J.A.; Hong, J.I., Fedorov, A.; Gole, J.L. Maintaining particle size in the transformation of anatase to rutile titania nanostructures. *Journal of Physics and Chemistry of Solids* **2008**, *69* (11), 2898–2906.
18. Ogawa, T.; Tsunetomi, E. Hot cracking susceptibility of austenitic stainless steels. *Welding Journal* **1982**, *61* (3), 82–93.
19. Goodwin, G.M. The effects of heat input and weld process on hot cracking in stainless steel. *Welding Journal* **1988**, *67* (4), 88–94.
20. Tseng, K.H.; Shiu, Y.J. Effect of thermal stability of powdered oxide on joint penetration and metallurgical feature of AISI 4130 steel TIG weldment. *Powder Technology* **2015**, *286*, 31–48.